Mongolian Geoscientist

Original Article

The heat flow losing via earth's surface around of Khulj hot spring

Shoovdor Tserendug[1*], Gendenpuntsag Bayanjargal[1], Tumen Nasan-Ochir[1], Tsoodol Zolbadral[2,3]

[1]*Department of Geomagnetism, Institute of Astronomy and Geophysics, Mongolian Academy of Sciences, Ulaanbaatar 13343, Mongolia*
[2] *Division of Nuclear Energy and Technology, Nuclear Research Center, National University of Mongolia, Ulaanbaatar 13330, Mongolia*
[3]*Department of General Science, New Mongolia Technology College, Ulaanbaatar 13372, Mongolia*

**Corresponding author: tserendug@iag.ac.mn, ORCID: 0000-0002-0594-4807*

ARTICLE INFO

***Article history*:**
Received 28 March, 2023
Revised 10 July, 2023
Accepted 29 August, 2023

ABSTRACT

In this paper, we extracted values of geomagnetic anomaly sourced in the lithosphere from the total intensity of geomagnetic that is measured on the 750 points on an area (100x100 km^2) around the Khulj hot springs. The two-dimensional map of the distribution of the anomaly geomagnetic corresponding to this area was made via these extracted values of anomaly geomagnetic. The method of spectral analysis was used to estimate the Curie Point Depth, which is lost magnetic characteristics of the lithosphere with a temperature of 580^o C and the depth of layer sourcing anomaly geomagnetic with high content of iron, nickel, and tungsten by these values of geomagnetic anomaly. On the Fig. 5, the isothermal Curie surface with the temperature of 580^o C was visualized in three dimensions by these values of Curie Point Depth. The heat flows lost on Earth's surface was also detected by the method of the gradient of temperature from the Curie Point Depth. And the two-dimensional map of heat flow around the Khulj hot spring was illustrated by the values of heat flows. Moreover, the average value of the heat flow for whole the area (100x100 km^2) was about 60 $[\frac{mW}{m^2}]$ and it was estimated at about 70 $[\frac{mW}{m^2}]$ at the Khulj hot springs. When we carried out a same study near Ulaanbaatar in 2018, the average heat flows lost on Earth's surface was determined about 40-50 $[\frac{mW}{m^2}]$.

Keywords: Curie point depth, Spectral analysis, Geomagnetic anomaly.

INTRODUCTION

The measured geomagnetic field on the Earth's surface is a summation of magnetics with many different sources. This study only focuses on the geomagnetic anomaly that originates in the lithosphere. In the lithosphere, there exist crystal rocks containing cobalt, nickel, and iron. Iron, cobalt, and nickel are substances with ferromagnetic properties. Briefly, the geomagnetic anomaly arises from the layer of the lithosphere contained with iron, cobalt, and nickel. In general, the temperature of the lithosphere is increased to the depth. The ferromagnetic properties of crustal rocks and minerals vanish in the crust's depth where the temperature is approximately 580^o C, or they

become a paramagnetic state. In other words, the geomagnetic anomaly arises from the rocks and minerals upper the boundary with a temperature of 580° C. The points with a temperature of 580° C are the critical points where the phase of crustal rocks and minerals is changed. The points of phase changed are called Curie points. Moreover, the distances from the earth's surface to the points, at which the phase of rocks is changed, are called Curie point depth (CPD).

The CPD could be estimated by the method of the spectral analysis of geomagnetic anomalies. The method of spectral analysis to define CPD was written briefly in this paper. Studies for CPD have been done indifferent countries' areas since 2000. For example, in the CPD for Macedonia and Thrace, N. Greece research is estimated range from 11.2 to 17.3 km. (Stampolidis and Tsokas, 2002). The CPD in central India is defined from 14 to 29 km (Bansal et al., 2013). The CPD in central Turkey is estimated about 13.7 km. (Nafiz, 2010). The CPD on the area (180x180 km^2) of North China is determined as the different values from 18 to 32 km. (Xu et al., 2017). The CPD on the island of Taiwan also ranges from 6 to 17 km (Hsieh et al., 2014). In addition, the heat flow lost on Earth's surface could be estimated by the method of the gradient of temperature from the CPD. We mentioned briefly the method of the gradient of temperature to define heat flow in this paper.

Previously, in 2018, our groups conducted a study to detect heat flows in two areas near Ulaanbaatar. The heat flows were determined about 40-50 $\left[\frac{mW}{m^2}\right]$ in these areas. The variation in the CPD could be occurred by the effects of geological activity phenomena such as activations of the tectonics and the volcanoes. No areas near to Ulaanbaatar that are obviously the result of geological activity were observed in our survey. There are many hot springs in the territory of Mongolia such as Khulj hot spring, Shargaljuut hot spring, and Tsetserleg hot spring. Therefore, Mongolian hot spring locations have attracted our attention for our next research. Thus, for this study, we focused on the region near the Khulj hot spring.This paper aims to estimate the heat flow losing Earth's surface around Khulj hot spring with latitude = 48.249259°, longitude = 102.953041°, and altitude=1472.2 m.

METHODOLOGY

Theoretically, $\Phi(k_x, k_y)$ is the power density spectrum of geomagnetic anomaly in the lithosphere is given by (Blakely, 1995) as

$$\Phi(k_x, k_y) = \Phi_M(k_x, k_y) \cdot F(k_x, k_y) \quad (1)$$

$$F(k_x, k_y) = 4\pi^2 C_m^2 |\theta_m|^2 |\theta_f|^2 e^{-2|k|z_t}(1 - e^{-2|k|(z_b - z_t)})^2 \quad (2)$$

where: $\Phi_M(k_x, k_y)$ -is the power density spectrum of magnetisation, $F(k_x, k_y)$ -is a function that depends on the vector directions of magnetisation and ambient field (Blakely, 1995). z_t -is the depth from the surface of Earth to the top of the magnetised layer. z_b -is the depth to the bottom of magnetised layer. C_m -is a constant. θ_m and θ_f -are factors related to the direction of magnetization and geomagnetic anomaly. k_x and k_y are the wavenumbers in the x and y directions, respectively. k is the horizontal wavenumber and is defined as follows

$$k = \sqrt{k_x^2 + k_y^2} \quad (3)$$

If the magnetization function, $M(x,y)$ -is completely random and uncorrelated, then $\Phi_M(k_x, k_y)$ -can be considered as a constant. The radial average values of θ_m and θ_f are constants and the factor of dependency on depth, $e^{-2|k|z_t}(1 - e^{-2|k|(z_b - z_t)})^2$ -is radial symmetry.

Thus, the radial average of $\Phi_M(k_x, k_y)$ can be written as following form

$$\overline{\Phi}(|k|) = A \cdot e^{-2|k|z_t}(1 - e^{-2|k|(z_b - z_t)})^2 \quad (4)$$

where: A -is a constant.

If taking quadrate root and natural logarithm of both sides of Eq. 4, it reformed into the following formula

$$\ln \overline{\Phi}(|k|)^{1/2} = \frac{1}{2}\ln(A) - |k|z_t + \ln(1 - e^{-2|k|(z_b - z_t)}) \quad (5)$$

If the wavelengths are less than approximately twice the thickness of the layer, Eq. 5 could be approached in the form

$$\ln \overline{\Phi}(|k|)^{1/2} = B - |k|z_t \quad (6)$$

where B -is a constant and equals with $\frac{1}{2}\ln(A)$.

Eq. 6 is used to estimate z_t -the depth to the top of a magnetic layer in many articles (Bansal, et al., 2013; Nafiz, 2010; Xu et al., 2017; Ngoh et al., 2020; Wen et al., 2019; Arnaiz-Rodríguez and Orihuela, 2013; Quintero et al., 2019; Audet and Gosselin, 2019).

We have also estimated the depth to the top of magnetic z_t from Eq. 6. If the centroid of magnetic layer (z_c) is expressed as

$$z_c = (z_b + z_t)/2 \quad (7)$$

Eq. 4 can be rewritten in the form

$$\overline{\Phi}(|k|) = A \cdot e^{-2|k|z_c}(e^{-|k|(z_t - z_c)} - e^{-|k|(z_b - z_c)})^2 \quad (8)$$

Moreover, the quadrate root of Eq. 8 could be obtained as

$$\overline{\Phi}^{\frac{1}{2}}(|k|) = C \cdot e^{-|k|z_c}(e^{-|k|(z_t - z_c)} - e^{-|k|(z_b - z_c)}) \quad (9)$$

Where C -is a constant and equals with $A^{1/2}$.

The values of distinctions $|z_t\text{-}z_c|$ and $|z_b\text{-}z_c|$ on the exponent in Eq. 9 are similar to the half the thickness of the magnetic layer (d) as

$$d = |z_t - z_c| = |z_b - z_c| \quad (10)$$

Thus, we can approach in Eq. 9 at long wavelengths as

$$\overline{\Phi}^{\frac{1}{2}}(|k|) = C \cdot e^{-|k|z_c}(e^{|k|d} - e^{-|k|d}) \approx C \cdot e^{-|k|z_c} \cdot 2|k|d \quad (11)$$

If we take the natural logarithm of $\overline{\Phi}^{1/2}(|k|)/|k|$ in Eq. 11, it can be rewritten in the following form

$$\ln\left(\overline{\Phi}^{1/2}(|k|)/|k|\right) = G - |k|\, z_c \quad (12)$$

where G -is a constant and equals with $ln(2Cd)$.

The centroid of magnetic layer z_c was estimated from Eq. 12 (Nafiz, 2010; Saleh et al., 2013; Xu et al., 2017; Ibrahim et al., 2022; Bilim et al., 2016; Guevara et al., 2013; Maus et al., 1997; Aydin et al., 2005). Thus, From Eq. 12, we have also estimated the centroid of magnetic layer z_c. In addition, the depth to the bottom of magnetised layer z_b is estimated as

$$z_b = 2z_c - z_t \quad (13)$$

The geothermal gradient (dT/dz) between the Earth's surface and the CPD (z_b) can be defined by Eq. 14 (Kassa et al., 2022; Aydin et al., 2005) and the Curie temperature for magnetic is at 580°C.

$$\frac{dT}{dz} = \frac{580^0 C}{z_b} \quad (14)$$

Additionally, the geothermal gradient can be related to the heat flow q by using the following formula (Nafiz, 2010; Xu et al., 2017; Hsieh et al., 2014).

$$\boldsymbol{q} = \lambda \frac{580^0 C}{z_b} \quad (15)$$

where λ -is the coefficient of thermal conductivity.

Eq. 15 demonstrates that the CPD is inversely proportional to the heat flow (Nafiz, 2010; Xu et al., 2017; Aydin et al., 2005; Salem et al., 2014; Avish et al., 2020; Harash and Chen, 2022).

Curie Point Depth and heat flow estimating around the Khulj hot spring

In 2022, we measured the absolute values of geomagnetic on the 700 points shown in Fig. 1 and the points, which are located by the matrix shape, are in the area (100x100 km^2)

surrounding the Khulj hot spring. The measured geomagnetic on the Earth's surface is a summation of the magnetic fields with many different sources.

The summation geomagnetic could be written as

$$B_1 = M_1 + (Br + Brv) + Ba_1 \quad (16)$$

where B_1 -is the absolute values of geomagnetic that are measured on the Erath's surface or on the points shown in Fig. 1. M_1 -is main geomagnetic that is sourced inner core of the Earth. B_r -is magnetic field that originates from outer of the Earth and B_{rv}-is its variation. Ba_1 -is geomagnetic anomaly that is sourced in the lithosphere. Ba_1 has local properties and it has to measure with different values on the points shown in Fig. 1.

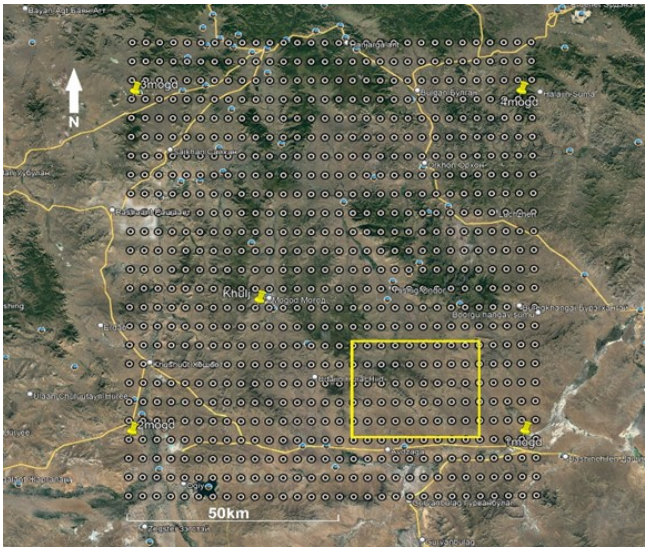

Fig. 1. Locations of points measured absolute values of the geomagnetic

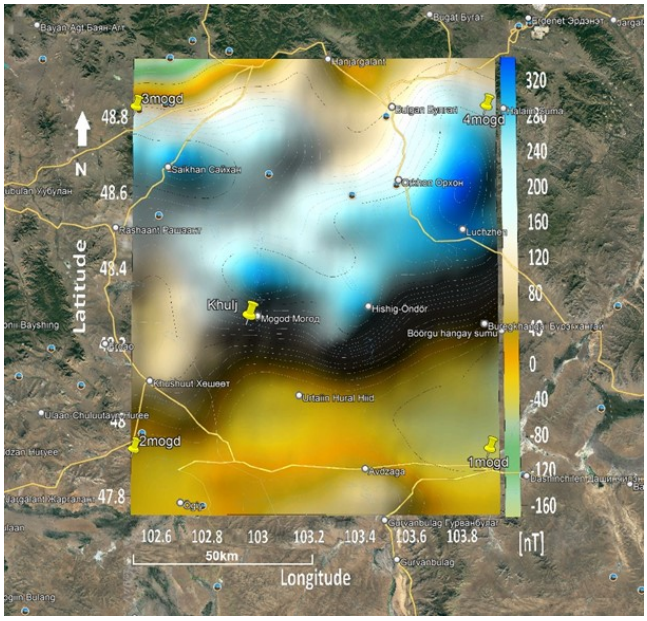

Fig. 2. The distribution of the geomagnetic anomaly could be illustrated by the expressed values in Eq. 19

The anomaly geomagnetic, originates from in the lithosphere, has to extract from the summation of the geomagnetic in Eq. 16. In order to extract the anomaly geomagnetic, we measured continuously the geomagnetic on stationary points among the area shown in Fig. 1.

The geomagnetic, which is measured on the stationary point, could be written as follows

$$B_0 = M_0 + (Br + Brv) + Ba_0 \quad (17)$$

From Eq. 17 the magnetic field, which is sourced outer of the Earth, and its variation could be rewritten as

$$(Br + Brv) = B_0 - M_0 - Ba_0 \quad (18)$$

The magnetic field in Eq. 18, which is sourced outer of the Earth, has global properties. As a result, we have attempted to measure the term (B_r+B_{rv}) in Eq. 18 with values that are similar to those on all of the points indicated in Fig. 1 at the synchronization moment.

From Eq. 16 and Eq. 18, the geomagnetic anomaly on the points in Fig. 1 can be written as

$$Ba_1 = B_1 - M_1 - (B_0 - M_0 - Ba_0) \quad (19)$$

where the terms M_1 and M_0 could be solved by the model IGRF on the points which latitudes, longitudes and altitudes are known. B_1 -is the value of the geomagnetic that is measured on the points in Fig. 1. B_0 -is the value of the geomagnetic that are measured on the stationary point synchronously with the points in Fig. 1. Ba_0 -is the geomagnetic anomaly on the stationary point and it is sourced in the lithosphere. According to our calculation, the value of the

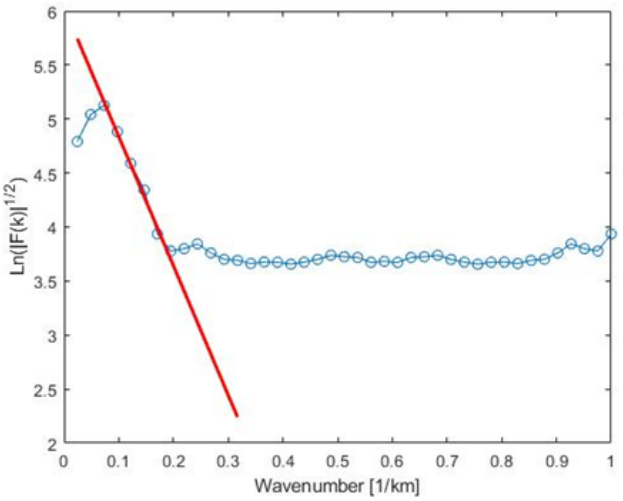

Fig. 3. The depth to the top of the source layer of strong magnetic, z_t by in Eq. 6 and this estimation is done performed at the center of yellow window shown in the Fig. 1.

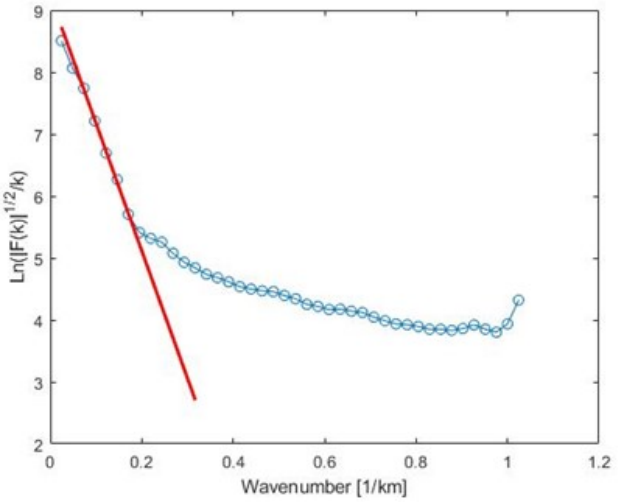

Fig. 4. The depth to the center of sourcing layer of strong magnetic, z_c by Eq. 12 and this estimation is done at the center of yellow window shown in the Fig. 1.

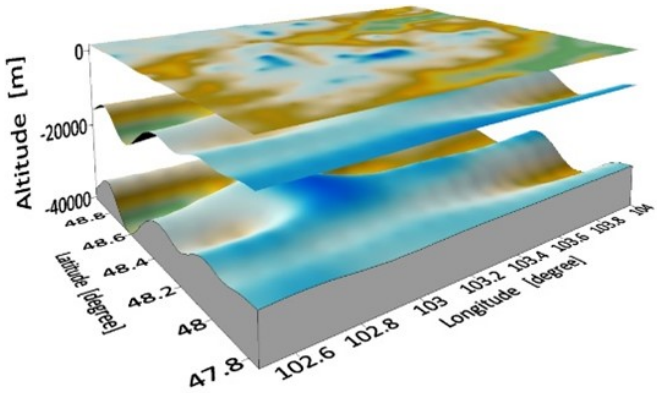

Fig. 5. The layers of CPD and top sourcing of magnetic anomaly are presented here. The Earth's surface is shown on the upper layer. The surface of top sourcing of geomagnetic anomaly is displayed on the middle layer and Curie surface is depicted on the bottom layer.

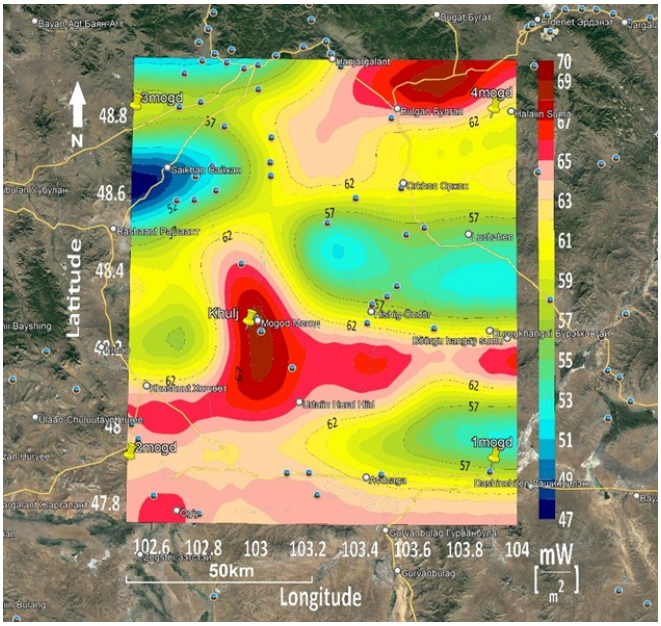

Fig. 6. The distribution of heat flow lost though the Earth's surface.

geomagnetic anomaly on the stationary point is about 89.5 nT.

The Distribution of the geomagnetic anomaly could be illustrated by the expressed values in Eq. 19 and it is shown on Fig. 2. For the area shown in Fig. 1, the power density depending on wave number on Eq. 6 could be solved by Fourier transform in the values of geomagnetic anomaly given by the Eq. 19.

In this case, the power density of dependency on the wave number in Eq. 6 could be solved by Fourier transform in the values of geomagnetic anomaly via Eq. 19 around the Khulj hot spring.

The angular coefficient of the linear part illustrated in Fig. 3 represents the depth to the top of the sourcing layer of the strong magnetic that it is z_t in Eq. 6. In the case shown in Fig. 3,

it is estimated as $z_t = \frac{6}{0.35} = 17.6$ km at the center of yellow border shown in the Fig. 1.

Similarly, the power density of the dependency on the wave number on the Eq. 12 could be solved and it is illustrated in Fig. 4. The angular coefficient of the linear part depicted in Fig. 4 represents the depth to the center of the sourcing layer of the strong magnetic that it is z_c in Eq. 12.

In the case of displayed in Fig. 4, it is estimated as $z_c = \frac{9}{0.35} = 25.7$ km at the center of yellow border shown in the Fig. 1.

Now, CPD, in which magnetic properties of the lithosphere are lost depth, could be solved from Eq. 13. On the occasion shown in Figs. 3 and 4, the CPD is solved as $z_b = 2z_c - z_t = 2 \cdot 25.7 - 17.6 = 33.8$ km.

Moreover, the heat flow, which is lost by the Earth's surface, could be solved by Eq. 15. Generally, the coefficients of thermal conductivity are $\lambda = 1.3 - 2.9 \left[\frac{W}{\text{m °C}}\right]$ in the layers of basalts and $\lambda = 2.4 - 3.8 \left[\frac{W}{\text{m °C}}\right]$ in the layers of granites (Nafiz, 2010; Xu et al., 2017; Hsieh et al., 2014).

The type of stone layers is commonly used to determine the values of the λ -coefficients in Eq. 15. In this case, the calculation was carried out in the yellow window in Fig. 1 behind the Avzaga Mountain. The granites predominates in the layer of stones close to the Avzaga. Therefore, λ -the coefficient of thermal conductivity was chosen as $\lambda = 3.3 \left[\frac{W}{\text{m °C}}\right]$

The heat flow, on the center of the yellow window in Fig. 1, equal to

$$q = \lambda \frac{580°C}{z_b} = 3.3 \frac{580}{33.8} = 56.2 \left[\frac{mW}{m^2}\right] \quad (20)$$

On the 250 central points, the CPDs and the heat flow for the whole area were studied by the method that transferred the yellow window according to the area (100x100 km^2) shown in Fig. 1.

The distribution map of the CPD for the studied whole area could be plotted by all the values of CPD. Similarly, the distribution map of heat flow for the whole area is presented via its all the values.

They are depicted in Figs. 5 and 6. The Earth's surface is shown on the upper layer in the Fig. 5. The surface of the top sourcing of the anomaly magnetic is displayed by the middle layer and Curie surface is also depicted by the bottom layer in Fig. 5. The distribution of the heat flow losing by the Earth's surface is depicted in Fig. 6.

RESULTS

The values of the geomagnetic anomaly are at about 200 - 300 nT at the center of the area and, is 10 - 80 nT for the southern part of the studied area. In the west-north of the area, which is around small lakes, the values of geomagnetic anomaly are at about -80 - -120 nT and it presented in Fig. 2.

The average CPD for the whole area was estimated at about -31.8 km. The CPDs nearby at the Khulj hot spring were about -27 - -29 km. In the part of the east-north of this area, the CPD were also defined at -27 - -29 km. The CPDs were about -33 - -40 km in the other part of this area. The values of heat flow were estimated at 65 - 70 $\left[\frac{mW}{m^2}\right]$ nearby at the Khulj hot spring. Generally, the values of heat flow were at about 63 - 65 $\left[\frac{mW}{m^2}\right]$ in the part of the west-south on the area shown in Fig. 6. In the part of the east-south and the east on the area, the values of heat flow were at about 51 - 61 $\left[\frac{mW}{m^2}\right]$

DISCUSSION

According to this study, the heat flow lost from

Earth's surface is detected relatively higher in the vicinity of the hot springs of Khulj than in other parts. In the northeastern part of this area, which is no surface water, there is a lot of heat flow as well. However, the heat flow is noticeably weaker in mountainous areas than other parts. The average heat flow for whole this area of (100x100 km^2) are estimated at about 60 $\left[\frac{mW}{m^2}\right]$ and the heat flow for this area varies in the 47-70 $\left[\frac{mW}{m^2}\right]$ range. Sulfur compounds are contained much in the hot springs of Khulj and this hot spring could be sourced by the extinct volcanic effects.

CONCLUSIONS

The negative values of the geomagnetic anomaly in the west-north of the area shown in Fig. 1 could be due to the effect of small lakes, and the direction of the ferromagnetic in rocks of the lithosphere, the opposite direction to the geomagnetic of Earth. According to this study, the average heat flow lost from Earth's surface is at about 60 $\left[\frac{mW}{m^2}\right]$ which is more heat flow than 40-50 $\left[\frac{mW}{m^2}\right]$ in areas in the vicinity of Ulaanbaatar. Moreover, the heat flow is at about 65-70 $\left[\frac{mW}{m^2}\right]$ nearby at the Khulj hot springs.

It means that the heat flow is relatively higher than the average for the whole area. It is observed that there exists also high heat flow in the small areas where there were no hot springs on the surface of the Earth.

REFERENCES

Arnaiz-Rodríguez, M.S., Orihuela, N. 2013. Curie point depth in Venezuela and the Eastern Caribbean. Tectonophysics, v. 590, p. 38-51. https://doi.org/10.1016/j.tecto.2013.01.004

Audet, P., Gosselin, J.M. 2019. Curie depth estimation from magnetic anomaly data: a re-assessment using multitaper spectral analysis and Bayesian inference. Geophysical Journal International, v. 218(1), p. 494-509. https://doi.org/10.1093/gji/ggz166

Avish, M.F., Ranjbar, H., Hojat, A., Karimi-Nasab, S. 2020. Curie point depth from spectral analysis of aeromagnetic data for reconnaissance exploration of geothermal potential; Case study: east of Kerman Province. Journal of the Earth and Space Physics, v. 46(1), p. 21-34. https://doi.org/10.22059/jesphys.2020.284503.1007134

Aydin, I., Karat, H.I., Kosak, A. 2005. Curie-point depth map of Turkey. Geophysical Journal International, v. 162, p. 633-640. https://doi.org/10.1111/j.1365-246X.2005.02617.x

Bansal, A.R., Anand, S.P., Rajaram, M., Rao, V.K., Dimri, V.P. 2013. Depth to the bottom of magnetic sources (DBMS) from aeromagnetic data of central India using modified centroid method for fractal distribution of sources. Tectonophysics, v. 603, p. 155-161. https://doi.org/10.1016/j.tecto.2013.05.024

Bilim, F., Akay, T., Aydemir, A., Kosaroglu, S. 2016. Curie point depth, heat-flow and radiogenic heat production deduced from the spectral analysis of the aeromagnetic data for geothermal investigation on the Menderes Massif and the Aegean Region, western Turkey. Geothermics, v. 60, p. 44-57. https://doi.org/10.1016/j.geothermics.2015.12.002

Blakely, R.J. 1995. Potential Theory in Gravity and Magnetic Applications. Cambridge University Press, 441 p. https://doi.org/10.1017/CBO9780511549816

Guevara, N.O., García, A., Arnaiz, M. 2013. Magnetic anomalies in the Eastern Caribbean. International Journal of Earth Sciences, v. 102, p. 591-604.

https://doi.org/10.1007/s00531-012-0828-6

Harash, F., Chen, C. 2022. Determination of Curie Point Depth Distribution and Heat Flow Regime Characteristics in Eratosthenes Seamount, Eastern Mediterranean Sea. Energies, v. 15(22), 8634. https://doi.org/10.3390/en15228634

Hsieh, H-H., Chen, C-H., Lin, P-Y., Yen, H-Y. 2014. Curie point depth from spectral analysis of magnetic data in Taiwan. Journal of Asian Earth Sciences, v. 90, p. 26-33. https://doi.org/10.1016/j.jseaes.2014.04.007

Ibrahim, A., Saada, S.A., Mickus, K., Abdelrahman, K., Khedr, F.I. 2022. Comparative study of estimating the Curie point depth and heat flow using potential magnetic data. Open Geosciences, v. 14(1), p. 462-480. https://doi.org/10.1515/geo-2022-0378

Kassa, M., Alemu, A., Muluneh, A. 2022. Determination of Conrad and Curie point depth relationship with the variations in lithospheric structure, geothermal gradient and heat flow beneath the central main Ethiopian rift. Heliyon, v. 8(11), e11735. https://doi.org/10.1016/j.heliyon.2022.e11735

Maus, S., Gordon, D., Fairhead, D. 1997. Curie-temperature depth estimation using a self-similar magnetization model. Geophysical Journal International, v. 129(1), p. 163-168. https://doi.org/10.1111/j.1365-246X.1997.tb00945.x

Nafiz, M. 2010. Curie-point Depth from Spectral Analysis of Magnetic Data in Erciyes Stratovolcano (Central TURKEY). Pure and Applied Geophysics, v. 167, p. 349-358. https://doi.org/10.1007/s00024-009-0017-0

Ngoh, J.D., Mbarga, T.N., Mickus, K., Tarek, Y., Tabod, T.C. 2020. Estimation of Curie Point Depth (CPD) across the Pan African Belt in Northern Cameroon from Aeromagnetic Data. Open Journal of Earthquake Research, v. 9(3), p. 217-239. https://doi.org/10.4236/ojer.2020.93013

Quintero, W., Campos-Enriquez, O., Hernandez, O. 2019. Curie point depth, thermal gradient, and heat flow in the Colombian Caribbean (northwestern South America). Geothermal Energy, v. 7, 16. https://doi.org/10.1186/s40517-019-0132-9

Saleh, S., Salk, M., Pamukcu, O. 2013. Estimating Curie point depth and heat flow map for Northern Red Sea Rift of Egypt and its surroundings, from aeromagnetic data. Pure and Applied Geophysics, v. 170, p. 863-885. https://doi.org/10.1007/s00024-012-0461-0

Salem, A., Green, C., Ravat, D., Singh, K.H., East, P., Fairhead, J.D., Mogren, S., Biegert, E. 2014. Depth to Curie temperature across the central Red Sea from magnetic data using the de-fractal method. Tectonophysics, v. 624-625, p. 75-86. https://doi.org/10.1016/j.tecto.2014.04.027

Stampolidis, A., Tsokas, G.N. 2002. Curie Point Depths of Macedonia and Thrace, N. Greece. Pure and Applied Geophysics, v. 159, p. 2659-2671. https://doi.org/10.1007/s00024-002-8752-5

Wen, L., Kang, G., Bai, C., Gao, G. 2019. Studies on the relationships of the Curie surface with heat flow and crustal struchures in Yunnan Province, China its adjacent areas. Earth, Planets and Space, v. 71, p. 85-104. https://doi.org/10.1186/s40623-019-1063-1

Xu, Y., Hao, T., Zeyen, H, Nan, F. 2017. Curie Point Depths in North China Craton Based on Spectral Analysis of Magnetic Anomalies. Pure and Applied Geophysics, v. 174, p. 339-347. https://doi.org/10.1007/s00024-016-1421-x